Available online at www.sciencedirect.com
ScienceDirect
International Journal of Mass Spectrometry 258 (2006) 13–20
International Journal of Mass Spectrometry
www.elsevier.com/locate/ijms

Cross flow ion mobility spectrometry: Theory and initial prototype testing

Mang Zhang [a,*], Anthony S. Wexler [a,b,c]

[a] Department of Mechanical and Aeronautical Engineering, University of California, Davis, CA 95616, USA
[b] Department of Civil and Environmental Engineering, University of California, Davis, CA 95616, USA
[c] Department of Land, Air and Water Resources, University of California, Davis, CA 95616, USA

Received 3 March 2006; received in revised form 17 May 2006; accepted 18 May 2006
Available online 19 June 2006

Abstract

By marrying the concepts behind ion mobility spectrometry (IMS) and differential mobility analysis (DMA), a new instrument, the Cross Flow Ion Mobility Spectrometer (CF-IMS) (patent pending), was constructed and tested. CF-IMS is a light-weight, low cost instrument that can analyze the composition of the gas phase continuously and with high mobility resolution. In this paper, we report the theory behind CF-IMS and measurements with a low resolution prototype. Reduced mobility of acetone, benzene, and pyridine at 473.15 K and 101.3 kPa were measured to be 2.35×10^{-4}, 2.32×10^{-4}, and 2.18×10^{-4}, $m^2\,V^{-1}\,s^{-1}$, respectively, in agreement with linear IMS measurements. CF-IMS could be used to analyze gas phase compounds or volatile particle phase compounds when used in conjunction with appropriate preconditioners.

Keywords: Ion mobility spectrometry; Aerosol

1. Introduction

A fast response, tough and simple instrument for toxic chemical, explosives, and biological agent detection in field situations is important for a range of applications. Various instruments [1] are available for real time analysis of potential pathogenic compounds. Most chemical analysis involves mass spectrometry, but mass spectrometry generally involves heavy, precise, and expensive equipment that is hard to use in the field. A common method for analyzing the chemical composition of airborne materials is with ion mobility spectrometry (IMS) since it operates in real time, is portable, and can distinguish many potentially harmful compounds, such as explosives and toxins, from benign ones. IMS is the leading technology for on-site detection of chemical warfare agents, explosives, and illicit drugs [2]. It is also the technology chosen by NASA for air quality monitoring aboard the International Space Station [3].

While IMS technology is constantly improving, mobility sizing of aerosol particles is also making significant strides. Charged particle velocities are inversely proportional to the effective collisional cross section of a charged particle, so electrical mobility classification by a differential mobility analyzer (DMA) is similar to molecular size analyses. A TSI scanning mobility particle sizer (SMPS) with a nano-DMA and nano-condensation particle sizer (CPC) can size and detect particles with mobility diameters as small as 3 nm. DMA mobility analysis assumes a constant source of charged particles with a range of mobilities.

Differential mobility analysis and ion mobility spectrometry balance drag and electrostatic force on particles or ions to separate them in space, thereby obtaining a mobility spectrum of the analyte. We have developed a mobility spectrometer (patent pending) that is able to analyze distributions of molecular ions, charged particles, and macromolecules or molecular clusters such as fresh nuclei that are between these two broad ranges. We call this device Cross Flow Ion Mobility Spectrometry (CF-IMS). Like a DMA, it is continuous because unlike conventional IMS, CF-IMS has no ion gate. In conventional IMS, the ions pass through a stagnant or near stagnant carrier gas—CF-IMS is more like a DMA in that the carrier gas (called a sheath gas in the DMA) is in motion. In conventional DMAs, faster sheath gas flows mean higher mobilities can be analyzed, so the ion mobility limit is governed by the transition to turbulence [4,5]. This analysis makes a crucial assumption that the characteristic length in the Reynolds number is the electrode spacing, which is true for conventional DMA geometries. Consider instead two

* Corresponding author. Tel.: +1 530 7544963; fax: +1 530 7544962.
E-mail address: mnazhang@ucdavis.edu (M. Zhang).

1387-3806/$ – see front matter © 2006 Published by Elsevier B.V.
doi:10.1016/j.ijms.2006.05.012

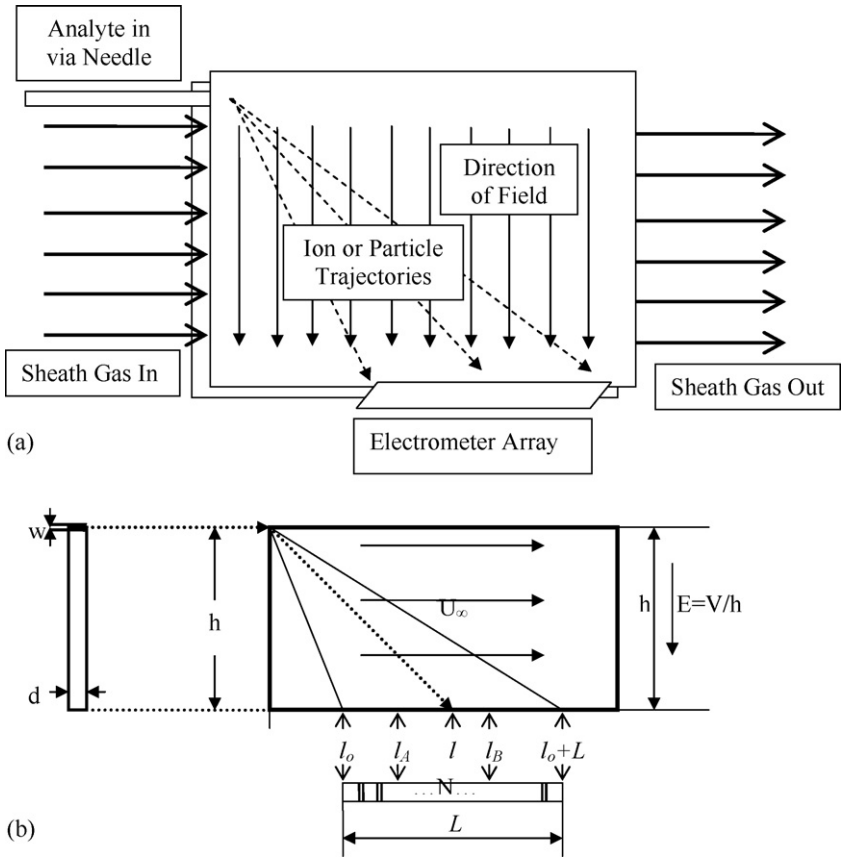

Fig. 1. Schematics of CF-IMS.

flat plates, as shown in Fig. 1, with a flow from left to right and an electric field forcing the ions from the entrance needle at the top left corner, through a sheath gas to an electrode array along the bottom. In this design, the characteristic Reynolds distance is the gap between the plates instead of the electrode spacing, so much higher sheath flow velocities can be attained while avoiding the transition to turbulence. This is akin to taking a pie slice out of a TSI EEPS or Cambustion DMS500. But taking a slice out of a DMA means that the volume flow rate may be that much smaller making sensitivity a potential concern. In CF-IMS this is alleviated with high sheath and source gas flow velocities, and ion or charged particle detection with an active pixel sensor (APS) array. APSs are becoming sensitive to as few as 100 e^-, with greater sensitivity promised [6,7]. For instance, 28 electron sensitivity at 0.3 Hz has been realized [8]. Megerle et al. [9] and Murphy et al. [10] invented miniature ion mobility spectrometers that employ one-dimensional or two-dimensional sensor arrays based on previous patents by Environics [11]. These designs have limited resolution due to absence of a sheath gas.

2. Theory

Electric mobility, Z, is defined by $u_{\text{drift}} = EZ$, where u_{drift} is the electrical migration velocity under the external electrical field E. The relationship between Brownian diffusivity, D, and electric mobility, Z, can be written as $Z = neD/kT = nD/v_{kT}$, a result known as the Einstein equation, where k is Boltzmann constant, T the absolute temperature, n the number of charges on the ion or particle, $v_{kT} = kT/e$, and e is the single electron charge. When gas ions and small particles with mobility diameter less than 10 nm are under consideration, a single charge assumption is usually valid, so $n = 1$. At room temperature, $v_{kT} = 0.0255$ V, which is used as a constant in what follows.

Consider the CF-IMS design schematic shown in Fig. 1, where the drawing shows the cross section of the CF-IMS cell with a rectangular sample needle inlet of width, w, that spans the cell gap, d. The sensor array, which also spans the cell gap, has N pixels with total length L. Sample is injected at position h. A uniform electric field, E, is imposed in the direction shown with a zero potential at the sensor array and a potential V at h. For our initial theoretical development, we will assume that the flow in the gap is uniform at a value of U_∞. Under the combined electrical field E and flow field U_∞, ions will strike position l on the sensor array, where l depends on the analyte electric mobility, Z. Constraints on the design are:

(1) the sheath and sample flows must be laminar to minimize dispersion of the ions and concomitant loss of resolution,
(2) sample and sheath air must have the same velocity when they merge to minimize eddy formation that also reduces resolution,
(3) the analyte should not diffuse more than the width of a single pixel on the sensor,

(4) the maximum field strength is limited by electrostatic breakdown to 10^4 V/cm,
(5) the sheath flow pressure drop must be as small as possible to minimize power consumption, and
(6) ion mobilities lie in the design range from Z_l to Z_h.

Higher flow rates are generally preferred because they decrease sample residence time, decrease diffusion loss and reduce sampling time as well as improve resolution, so the maximum sheath flow velocity is desired. The flow velocity is limited by the transition to turbulence (see point 1 above) which occurs at a Reynolds number of about 2300 [12], where $\mathrm{Re} = U_\infty D_h/v$, $D_h = 2d$ is the hydraulic diameter and v is the kinematic viscosity of the sheath gas, which at room temperature and pressure is 0.16×10^{-4} m^2/s since the sheath gas is air. Thus, the laminar flow limitation gives

$$U_\infty d \leq \frac{2300v}{2} = 0.0184\,\mathrm{m}^2/\mathrm{s} \tag{1}$$

Using point 2 above, the sample flow rate through the needle is $Q_a = U_\infty dw$, the sheath air flow rate is $Q_s = U_\infty dh$, and their ratio is $Q_s/Q_a = h/w$. The time for the sample ions to pass from the needle exit to the sensor array is $t = h/EZ$. The diffusion distance δ_x can be expressed as

$$\delta_x = \sqrt{2Dt} = \sqrt{2v_{kT}Z\frac{h}{EZ}} = \sqrt{2v_{kT}\left(\frac{h}{E}\right)} = h\sqrt{\frac{2v_{kT}}{V}} \tag{2}$$

which shows that in CF-IMS (a) the diffusion distance is independent of the analyte mobility and (b) higher field strengths, E, and smaller cell dimensions, h, give lower analyte diffusion and therefore higher mobility resolution. Thus, the maximum electrical field strength, determined by breakdown, sets the diffusion distance.

There are four mechanisms that limit resolution in CF-IMS: The width of the sample needle, w, the diffusion distance, δ_x, the pixel size, and dispersion due to non-uniform sheath flow. We set the needle width, diffusion distance and pixel size equal to each other to evenly distribute these sources of ion position uncertainty (discussed in more detail below). Setting the diffusion distance, δ_x, equal to the sensor pixel size N/L (point 3 above), where N is total pixel number and L is the sensor length, the ratio of cell height to field strength is given by:

$$\frac{h}{E} = \frac{\delta_x^2}{2v_{kT}} \tag{3}$$

Analyte with mobility Z will strike position l on the electrometer array, such that

$$l = \frac{h}{Z(V/h)}U_\infty \tag{4}$$

where $Z(V/h)$ is the ions migration velocity under the electrical field $E = V/h$. If we design a CF-IMS configuration to detect analytes over a mobility range Z_l–Z_h using a sensor of length L, then, $hU_\infty/EZ_h = hU_\infty/EZ_l + L$ which when combined with Eq. (2) gives:

$$U_\infty = L\frac{2v_{kT}}{\delta_x^2}\left(\frac{Z_hZ_l}{Z_h - Z_l}\right) \tag{5}$$

Similar to Knutson and Whitby [13] and Flagan [14], the ability of the CF-IMS to resolve mobility can be expressed in terms of the ratio of the mobility at peak transmission efficiency to the full width at half maximum (FWHM) of this transfer function, $R = Z^*/\Delta Z_{\mathrm{FWHM}}$. Resolution in CF-IMS is governed by the needle dimension, w, the analyte diffusion distance, δ_x in Eq. (2), and the pad size on the sensor array, L/N. Let us examine how the resolution depends on pad size by temporarily ignoring diffusion. From the geometry of Fig. 1b, analyte with mobility Z^* strikes a sensor pad whose width is $\Delta l = L/N$ at position $l = hU_\infty/EZ^*$. The minimum analyte $Z_{\min}$ that leaves the needle and reaches the pad centered at l leaves the bottom of the needle slit at vertical position $h - w/2$ and strikes the far right side of the pad at horizontal position $l + \Delta l/2$. Likewise, the maximum mobility, $Z_{\max}$, leaves the needle slit at $h + w/2$ and strikes the pad at $l - \Delta l/2$, so that

$$\begin{aligned} l + \frac{\Delta l}{2} &= \frac{(h - w/2)U_\infty}{EZ_{\min}} \\ l - \frac{\Delta l}{2} &= \frac{(h + w/2)U_\infty}{EZ_{\max}} \end{aligned} \tag{6}$$

after combining these equations with $l = hU_\infty/EZ^*$ and defining $R = Z^*/(Z_{\max} - Z_{\min})$, we obtain:

$$R^{-1} = \frac{w}{h} + \frac{\Delta l}{l} \tag{7}$$

where in the derivation, we assumed that $\Delta l \ll l$. So small w and Δl give higher resolution, both of which may limit CF-IMS sensitivity since smaller needles inject fewer ions into CF-IMS and smaller pads receive fewer ions and therefore less current. Since the optimum values depend on the analyte concentration range, ionization efficiency, sensor array characteristics, and other parameters that are specific to a given application, we will make the simplify assumption that $l = h$ and $w = \Delta l$ to evenly distribute resolution over these two effects illustrating one possible CF-IMS design. Note that in Eq. (7), the resolution is a function of the analyte mobility, because $l = l(Z)$ and Δl is fixed.

In the derivation of Eqs. (6) and (7), we assumed that the diffusion distance was small to illustrate the particle trajectories and their associated limitations on resolution. Now let us improve Eq. (6) by adding the diffusion distance from Eq. (2) to the geometric factors, to obtain:

$$\begin{aligned} l + \left[\frac{\Delta l}{2} + \delta_x\frac{\sqrt{h^2 + l^2}}{h}\right] &= \frac{(h - w/2)U_\infty}{EZ_{\min}} \\ l - \left[\frac{\Delta l}{2} + \delta_x\frac{\sqrt{h^2 + l^2}}{h}\right] &= \frac{(h + w/2)U_\infty}{EZ_{\max}} \end{aligned} \tag{8}$$

which when solved with the definition of resolution becomes

$$R^{-1} = \frac{w}{h} + \frac{\Delta l}{l} + \frac{2\delta_x\sqrt{h^2 + l^2}}{hl} \tag{9}$$

Table 1
Design Parameters for CF-IMS

Prototypes	High resolution	Low resolution
Dimension L × W × H (m)	0.2 × 0.1 × 0.001	0.025 × 0.025 × 0.0016
Sample flow rate × 10^6 (m^3/s)	4.2	5
Sheath gas flow rate × 10^3 (m^3/s)	1.8	5×10^{-2} to 8.3×10^{-2}
Recirculation blower power (W)	0.8	≪1
Mobility range ($m^2\,V^{-1}\,s^{-1}$)	0.015–0.03	0.01–0.025
Molar mass range (Da)	30–600	30–600
Sample flow pressure drop (Pa)	64	<1
Sheath flow pressure drop (Pa)	435	<1
Power supply voltage (kV)	10	5
Sensor length (m)	0.1	0.02.54
Electrometer pad size × 10^3, $L \times d$ (m × m)	0.2 × 1	0.8 × 1.6
Mobility resolution	92	10

Again, $l = h$ and $w = \Delta l = 2\delta_x$ will evenly distribute resolution over those three effects: needle width w, sensor width Δl, and diffusion distance δ_x.

Note that mobility resolution can be related to mass resolution as follows. Tammet [15] provides a relationship between analyte reduced mobility and mass, which can be written as $Z = 14/m^{1/3}$, so that mass resolution R_m can be related to mobility resolution by:

$$R_m = \frac{m}{\Delta m} = \frac{1}{3}\frac{Z}{\Delta Z} = \frac{R}{3} \tag{10}$$

From Eq. (9), higher CF-IMS height, h and length, l, lead to higher resolution. Is there a limitation? From constraint point 4, in order to analyze an ion with mobility Z with the maximum resolution, the sheath velocity will be $U_\infty = EZ$ where E is the maximum breakdown electrical field. To satisfy constraint point 1 or Eq. (1), gap distance must be $d = Rev/2U_\infty$. Given the CF-IMS height h, we know that l should be at least about h to evenly distribute resolution loss over the various effects (Eq. (9)). Choosing the total CF-IMS length L equal $2h$ or $2l$ and $w = \Delta l = 2\delta_x$, we can calculate the voltage $V = Eh$, resolution from Eq. (9), sample flow rate from $Q_a = U_\infty dw$, sheath flow rate from $Q_s = U_\infty dh$, and sample pressure drop from

$$\Delta P_a = \frac{12\mu L_{\text{needle}}}{dw^3} Q_a = \frac{12\mu L_{\text{needle}} U_\infty}{w^2} \tag{11}$$

Here μ is air viscosity, L_{needle} is needle length. Note that $w^2 = (2\delta_x)^2 = 8v_{kT}h/E$. Likewise, the sheath pressure drop is:

$$\Delta P_s = \frac{12\mu L}{hd^3} Q_s = \frac{12\mu L U_\infty}{d^2} \tag{12}$$

From Eq. (11), ΔP_a is inversely proportional to h which means sample pressure drop increases rapidly as h becomes small. From Eq. (12), ΔP_s is proportional to h which means that sheath pressure drop increases linearly with h. Also remember applied voltage increases with h and since the maximum field strength is 1000 kV/m, $h = 0.1$ m requires a 100 kV power supply.

Considering all the constraints placed on the CF-IMS design by the aforementioned equations and considerations, the optimum design depends on a range of trade-offs. Table 1 lists two proposed CF-IMS designs, one high resolution and one low resolution design, tests of which are presented here. In Table 1, the single pad current is based on a molecule ionization efficiency of 10^{-6} [16] and is given for the stated analyte concentrations.

3. CF-IMS prototype

We have built and tested a prototype of CF-IMS using a ^{63}Ni ionization source. In these tests, common organic (e.g., acetone, pyridine, benzene) compounds were sampled at different conditions to understand their analysis with CF-IMS. Also mixtures were analyzed. Since a sensor array was not available, we built a low-resolution CF-IMS prototype. The flows, voltages and geometry of CF-IMS listed in Table 1, column 3, were still optimized for experimental conditions that were available in our laboratory without employing the sensor array.

The CF-IMS cell (Fig. 2) consisted of two parallel printer circuit boards (PCBs) with leads etched on their surfaces that were precisely aligned with a flip chip bump bonder—the leads impose the electric field, E, in the cell. Each PCB had 25 0.25×10^{-3} m metal traces with 0.76×10^{-3} m gaps between

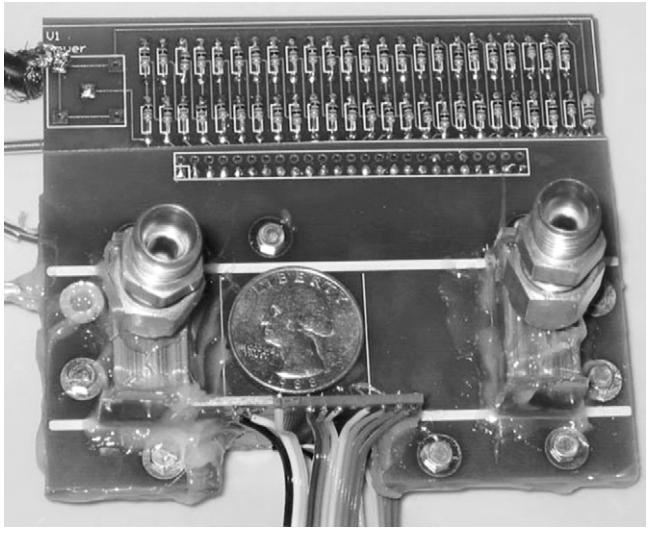

Fig. 2. Prototype of low resolution CF-IMS with 0.05 m × 0.05 m × 8×10^{-4} m drift cell formed by two parallel printed circuit boards.

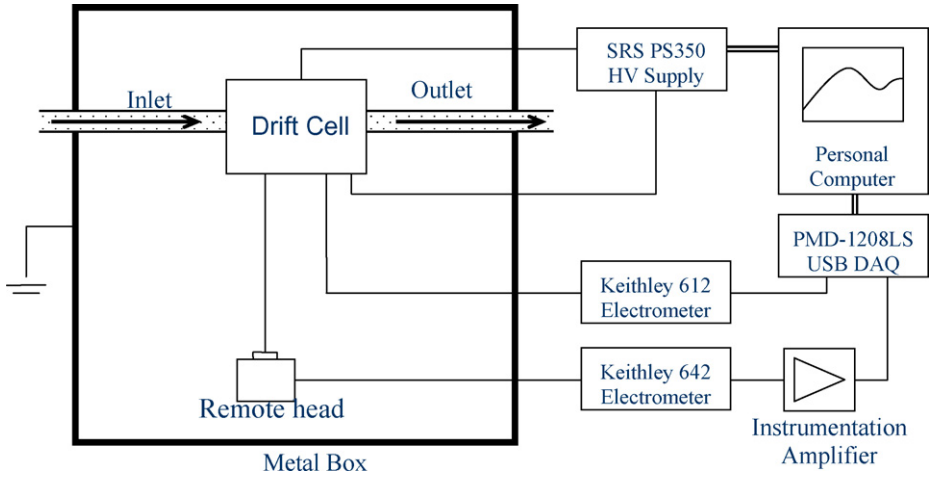

Fig. 3. CF-IMS test configuration.

them forming a 25.4×10^{-3} m by 25.4×10^{-3} m drift region. The PCBs were spaced 1.6×10^{-3} m apart.

Fifty 10 MΩ carbon film resistors (Yageo) connect the leads and provide a voltage divider. Inlet and outlet sheath gas manifolds are bonded to the PCBs and provide a Swagelock connection to the sheath gas supply lines. A 1/16″ aluminum tube (upper left corner of the PCB) serves as the sample inlet. The sensor board had 25 0.76×10^{-3} m wide uncoated metal pads with 0.25×10^{-3} m space between each pad. The pads spanned the 1.6×10^{-3} m gap.

Dry air (<1 ppm) from the Zero Air cylinder was split into sample flow and sheath flow. Flow rates were controlled by a mass flow controller and monitored by a mass flow meter. Both flows passed through a moisture trap, hydrocarbon trap, and HEPA filter. Sample flow also passed by a diffusion cell with a capillary tube neck diffusion vial, which was filled with analyte. At room temperature, 295 K, and a specific carrier air flow rate, a constant analyte concentration is obtained by chemical diffusion. Estimated concentration of acetone, pyridine, benzene were 5, 3, and 3 ppm, respectively. The diffusion cell could hold up to 2 vials for samples mixtures. Before the sample flow was introduced into the CF-IMS needle, it was ionized by a 20 mCi ^{63}Ni beta source.

For most of the tests reported here, two electrometers recorded current from two of the pads while the others were connected to ground. The CF-IMS cell, ionization cell and remote head of the Keithley 642 electrometer (Fig. 3) were placed in a sealed and grounded metal box to shield against electrical noise. Sample, sheath, exhaust flow tubing, and electrical wires were carefully introduced through the box walls and thoroughly shielded.

A personal computer with Labview® controlled a SRS PS300 power supply via a GPIB interface and read data from two electrometers via a Measurement Computing PMD-1208LS USB-based DAQ. Since only two electrometers were available, the cell voltage was scanned to test the instrument. Voltages increased from 50 to 3000 V in steps of 10 V. The time between each step was 10 s to allow time for the electrometers to settle. Electrometer sample rate was set at 2 Hz and the initial 10 data points recorded after a voltage change were discarded. Subsequent readings from the electrometers was averaged and saved as filtered current readings.

Before each experiment, the system was run at experimental condition for at least 30 min without applied voltage in order that the diffusion cell and ionizer could achieve equilibrium. Every electrical instrument also was power on at least 3 h prior to use to minimize warm-up transients.

4. Measurements

Mobilities of acetone, pyridine, benzene, and their mixtures in air were measured; literature values are listed in Table 2, measurements in Table 3. In Fig. 1b, l_A and l_B are the horizontal distance between the needle and center of pads A and B where the electrometers recorded current. For the spectra recorded here, current was detected as a function of voltage. The voltage at peak pad current satisfies

$$l_A = \frac{h}{Z(V_A/h)}U_\infty \qquad l_B = \frac{h}{Z(V_B/h)}U_\infty \tag{13}$$

where V_A and V_B are peak voltages from the electrometer pads A and B, respectively. For example, V_A is the applied voltage that results in the peak of the ion trajectory striking position l_A, the location of electrometer pad A. Regardless of the analyte,

Table 2
Molar masses and mobilities ($m^2\ V^{-1}\ s^{-1}$) of analytes

Chemical name	Molecular weight (amu)	Reduced mobility × 10^4
Air	29	1.90,1.93,1.89 [2]* 2.09 [17]
Pyridine	79	2.21 [2]*
Acetone	58	2.33 [2]*
Benzene	78	2.31 [2]*

* Reduced mobility at 473.15 K and 101.3 kPa.

Table 3
Mobility ($m^2\ V^{-1}\ s^{-1}$) measured by CF-IMS

	Experimental mobility ratio		Experimental mobility ratio	Literature [2] mobility ratio
Air/acetone	1.272	Pyridine/acetone	0.930	0.948
Air/benzene	1.286	Acetone/benzene	1.011	1.009
Air/pyridine	1.369	Pyridine/acetone	0.939	0.957

Experimental reduced mobility $\times 10^4$ under 473.15 K and 101.3 kPa

Acetone	2.35
Benzene	2.32
Pyridine	2.18

we can see from Eq. (13) that:

$$\frac{l_B}{l_A} = \frac{V_A}{V_B} = \text{Const.} \tag{14}$$

as long as U_∞ remains fixed, where $l_B/l_A = 3.4$ in the configuration presented here. Fig. 4 shows measured V_A/V_B values for purified air, acetone, benzene, pyridine, and their mixtures. The numbers in parentheses in the legend are standard deviation for each chemical species. The horizontal line in Fig. 4 represents the measured average value 3.5 from over 60 data points. The standard deviation was +3% compared with theoretical value 3.4.

For the same analyte under different sheath flow velocities, the voltage that gives the peak pad current (referred to as peak voltage from now on) is given by:

$$l = \frac{h}{Z(V_I/h)}U_\infty = \frac{h}{Z(V_{II}/h)}U_{\infty II} \Rightarrow \frac{V_I}{V_{II}}\frac{U_{\infty II}}{U_{\infty I}} = 1 \tag{15}$$

where V_I and V_{II} are peak voltages corresponding to sheath flow velocities, $U_{\infty I}$ and $U_{\infty II}$, respectively. Fig. 5 shows values of $(V_I/V_{II})(U_{\infty II}/U_{\infty I})$ for 54 data points, confirming that peak voltage is inversely proportional to sheath flow velocity as suggested by the governing equations. As in Fig. 4, the numbers in parentheses in the legend are standard deviations for each analyte.

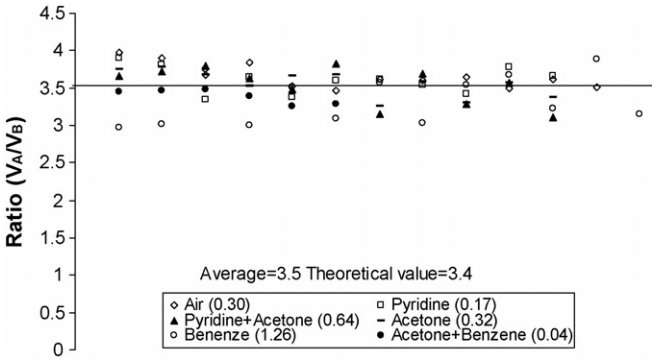

Fig. 4. Measured voltage ratio (at peak pad current) at position A and B for purified air, pyridine, acetone, benzene and their mixtures; numbers in parenthesis are standard deviations.

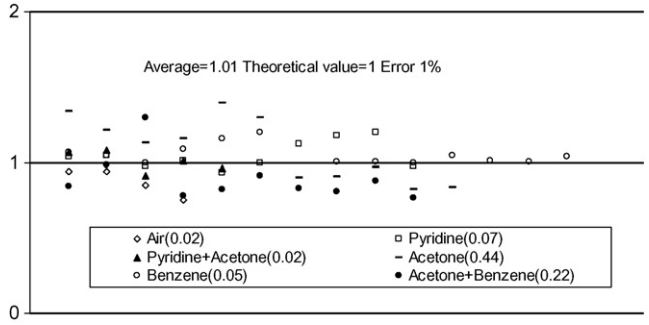

Fig. 5. Measured $(V_I/V_{II})(U_{\infty II}/U_{\infty I})$ values at the same position for purified air, pyridine, acetone, benzene and their mixtures; numbers in parenthesis are standard deviations.

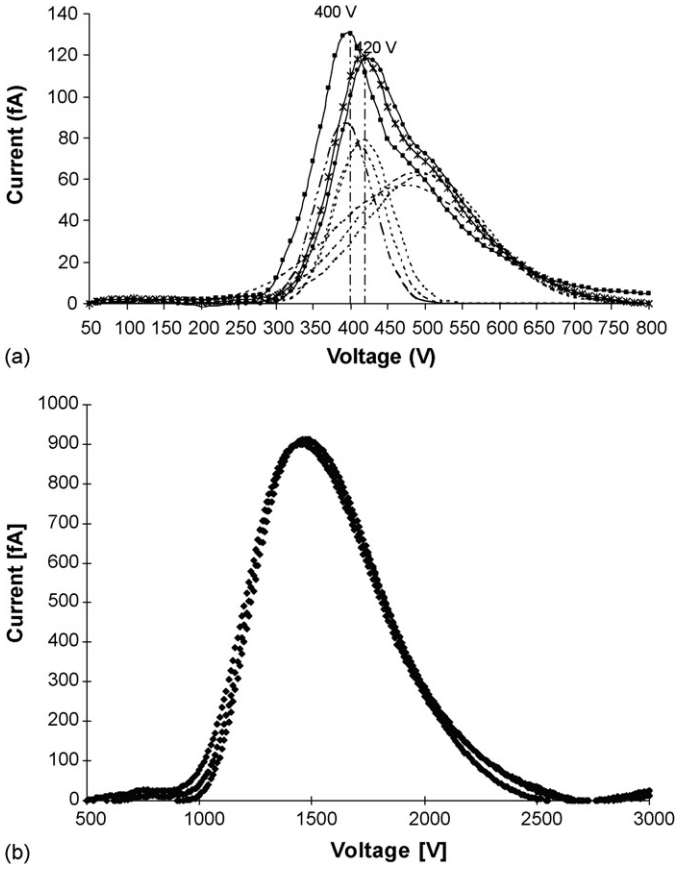

Fig. 6. (a) Measured current vs. applied potential at sensor position A for purified air. Symbols represent different runs; dashed lines represent normalized fits to the data. (b) Measured current vs. applied potential at sensor position B for purified air. Symbols represent different runs.

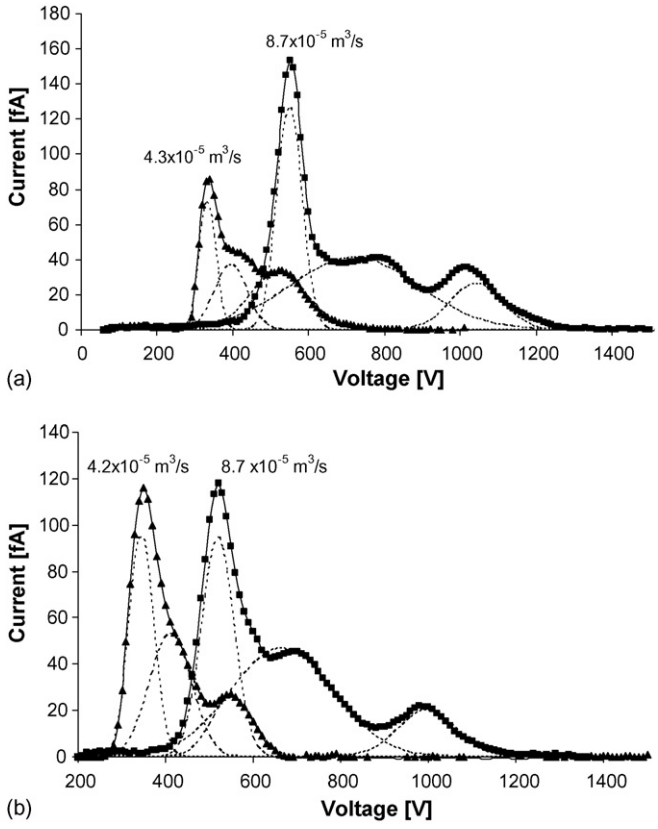

Fig. 7. (a) CF-IMS scanning spectra for a mixture of acetone and benzene showing sheath flow rate variation. Symbols represent different sheath flow rate; dashed lines represent normalize fits to the data. (b) CF-IMS scanning spectra for acetone showing sheath flowrate variation. Symbols represent different sheath flow rates; dashed lines represent normalize fits to the data.

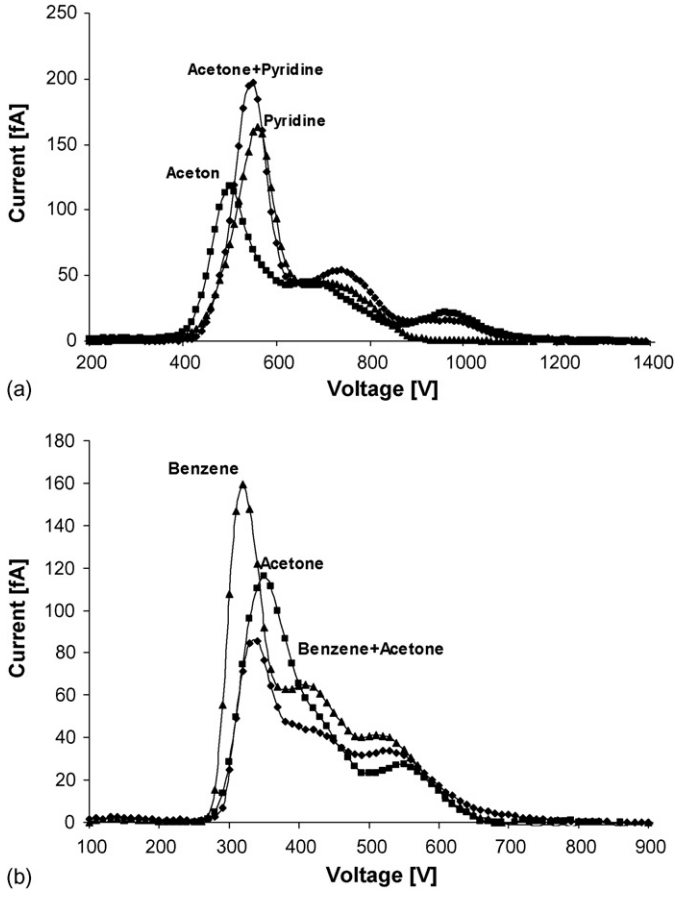

Fig. 8. (a) CF-IMS scanning spectra for acetone (square), pyridine (triangle) and their mixture (diamond) under the same operating conditions. (b) CF-IMS scanning spectra for acetone (square), benzene (triangle) and their mixture (diamond) under the same operating condition.

Figs. 6–8 show measured pad current versus scanning voltage. Here current noise drift due to leakage under high applied potential has been subtracted. Dashed lines in Figs. 6a, 7a, and 7b were fitted by Eq. (16).

$$I = \sum_i \frac{A_i}{\sigma_i \sqrt{\pi/2}} \mathrm{e}^{\frac{-2(V-V_{i,\mathrm{peak}})^2}{\sigma_i^2}} \tag{16}$$

where A_i is the peak amplitude, $V_{i,\mathrm{peak}}$ the peak voltage and $V_{i,\mathrm{FWHM}}$ the full width half maximum voltage, such that $V_{i,\mathrm{FWHM}} = 1.177\sigma_i$.

Fig. 6a and b show three consecutive runs, 6a corresponding to position A and 6b corresponding to B. Curves which represent consecutive runs overlap very well. The deviation of the peak voltage value was less than 20 V. Note that the voltage step was 10 V. From the curve, resolution was the peak voltage divided by the fitted Gaussian curve half width $V_{i,\mathrm{FWHM}}$. In Fig. 6a and b, the fitted peak voltages were 407 and 1530 V, respectively; $V_{i,\mathrm{FWHM}}$ values were 648 and 85 V, respectively, corresponding to a resolution of 2.4 and 4.9, respectively. Theoretical resolution from Eq. (9) predicts a resolution of 3.4 at position A and 8.6 at position B. Observed values were about 70% at position A and 60% at position B of the diffusion prediction. Signal strength from position B was lower than position A because the increased travel time and distance causes ion loss to the PCBs due imperfect alignment of the boards and diffusion.

Despite the lower signal strength of position B, we choose position B for further investigation since it had higher resolution and it required lower applied voltages. Fig. 7a and b show the effect of sheath flow changes with the same needle flow rate. Fig. 7a represents an acetone and benzene mixture. Fig. 7b represents acetone. Ion mobility spectra of acetone from the literature also show three peaks [17]. The first peak is the reaction ion peak (RIP), the second peak is analyte monomer and the third peak is analyte dimer. The reaction ion peak is produced by positive air ions N_2^+, H_3O^+, and their combination. Peaks in Fig. 8a were charged air, pyridine monomer and pyridine dimer. Peaks in the Fig. 8b were positive air ions, acetone monomer ions and acetone dimer ions. Air ions have a much higher concentration than analyte so produce a higher signal, as expected. Both figures show a slight resolution increase with sheath flow rate increase. The resolution of the first peak in Fig. 7a increases from 6.56 to 7.13, which agrees with the theoretical analysis in that higher sheath velocity gives shorter ion residence time and less ion diffusion broadening. The relatively stronger signal strength also suggested

less ions loss due to diffusion. Note how the second peak in Fig. 7b is more easily identified under higher sheath flow conditions.

Fig. 8a shows measurements for acetone, pyridine and their mixture at sheath flow rate of about 8.3×10^{-5} m^3/s. Fig. 8b shows data for acetone, benzene and their mixture at a sheath flow rate around 4.2×10^{-5} m^3/s. Three peaks can be identified for every analyte and their mixture. From Fig. 8a, peak voltage of pyridine and acetone mixture lies between that of pyridine and acetone.

5. Conclusion

Unlike the traditional ion mobilities spectrometers and differential mobility analyzers, Cross Flow Ion Mobility Spectrometry (CF-IMS) uses a parallel plated configuration and higher flow velocity by decreasing the characteristic dimension in the Reynolds number to achieve higher resolution. Its electrometer sensor array eliminates voltage scanning in the DMA and the shutter gate in IMS, both of which decrease duty cycle in these instruments. A simple prototype CF-IMS exhibited good agreement with theory and measured mobility values in agreement with those measured by conventional IMS (Table 3). Eventually, CF-IMS could be used to analyze the gas and/or particle phase constituents of the aerosol. Since the particles have low mobility, if the aerosol is introduced into CF-IMS, the particles will pass out with the sheath and not affect the signal. By denuding the gas first and then heating the remaining particles to evaporate the volatile components into the gas phase, the volatile particle-phase components may be analyzed. Other pre-conditioners can be used for a wide range of other purposes.

Acknowledgment

Support for this work was provided by Camille and Henry Dreyfus Postdoctoral Program in Environmental Chemistry and the California Energy Commission PIER program. The author acknowledges the assistance from Paul Gomez and Richard Lander for bump bonding the printed circuit board.

References

[1] P.A. Baron, E. Willeke, Aerosol Measurement: Principles, Techniques and Applications, second ed., Wiley Interscience, 2001.
[2] G.A. Eiceman, Z. Karpas, Ion Mobility Spectrometry, CRC Press, Baton Rouge, 1993.
[3] E.S. Reese, S.J. Taraszewski, T.F. Limero, J.T. James, Eighth International Conference on Ion Mobility Spectrometry, 1999.
[4] F.J. Gomez-Moreno, J. Rosell-Llompart, J. Fernandez de la Mora, J. Aerosol Sci. 33 (2002) 459.
[5] R.C. Flagan, Aerosol Sci. Technol. 30 (1999) 556.
[6] S. Fuerstenau, G. Soli, T. Cunningham, B. Hancock, B. Pain, M. Sinha, Int. J. Mass Spectrom. 215 (2002) 101.
[7] A.K. Knight, R.P. Sperline, G.M. Hieftje, E. Young, C.J. Barinaga, D.W. Koppenaal, M.B. Denton, Int. J. Mass Spectrom. 215 (2002) 131.
[8] P.S. Riehl, Micromachined resonant electrometer. Unpublished Master Thesis University of California at Berkeley, 1999 p. 96.
[9] C.A. Meagerle, C.W. Townsend, J.F. Linders, Raytheon Company, US Patent 5,965,882, 1999.
[10] J.B. Murphy, C.A. Megerle, C.W. Townsend, Raytheon Company, US Patent 6,630,663 B2, 2003.
[11] P. Puumalainen, Environics, Oy, US Patent 5,047,723, 1991.
[12] F.M. White, Fluid Mechanics, second ed., McGraw-Hill, 1988.
[13] E.O. Knutson, K.T. Whitby, J. Aerosol Sci. 6 (1975) 443.
[14] R.C. Flagan, Aerosol Sci. Technol. 38 (2004) 890.
[15] H. Tammet, J. Geophy, Res. Atmos. 103 (1998) 13933.
[16] M. McKeown, M.W. Siegel, Am. Lab. 7 (1975) 89.
[17] P. Watts, Anal. Proc. 28 (1991) 325.